Max-Planck-Institut
für Mathematik
in den Naturwissenschaften
Leipzig

# Domain Configurations in Soft Ferromagnetic Films under External Field

by

*Lukas Döring, Elias Esselborn, Samuel Ferraz-Leite, and Felix Otto*

Preprint no.: 3 2012

# Domain Configurations in Soft Ferromagnetic Films under External Field ⋆

**L. Döring, E. Esselborn, S. Ferraz-Leite, F. Otto**

*Max Planck Institute for Mathematics in the Sciences, Inselstraße 22, 04103 Leipzig, Germany, (e-mail: samuel.ferraz-leite@mis.mpg.de).*

**Abstract:** This note is about the prediction of the domain and wall configuration formed by the magnetization $\mathbf{m}$ in a soft ferromagnetic film under an external field. We propose a modification of the reduced model introduced by DeSimone et al. (2001), that is a variational model for a 2-d in-plane magnetization $\mathbf{m}$ on the cross section $\omega$. The modification consists of two parts:

1.) An unphysical but computationally convenient selection criterion in DeSimone et al. (2001) is replaced by a selection criterion based on physical wall energy,
2.) The set of admissible configurations is restricted by imposing an additional boundary condition at the boundary $\partial\omega$ of the cross section.

The specific wall energy is computed off-line based on a 2-d reduction of the 3-d model from Döring et al. (2012b), and then fed into a diffuse interface approximation for the selection criterion 1.). This retains some of the low complexity of the original model DeSimone et al. (2001). Modification 2.) allows to model hysteresis as observed in experiments by van den Berg and Vatvani (1982); preliminary numerical simulations reveal good qualitative agreement.

*Keywords:* Thin-film micromagnetics, magnetic domains, wall energy

## 1. INTRODUCTION

Our work deals with the simulation of pattern formation in soft (i.e. low-anisotropy) ferromagnetic films. Starting point is the widely accepted continuum model due to Landau and Lifschitz (1935): Consider a cylindrical ferromagnetic sample $\Omega = \omega \times (0,t)$ with diameter $\operatorname{diam}(\Omega) \sim 1$ and $t \ll 1$. Its magnetization is a vector field $\mathbf{M}\colon \Omega \to \mathbb{R}^3$ of constant length $|\mathbf{M}| = 1$. We apply a constant external field $\mathbf{H}_{\rm ext}$. The micromagnetic free energy, in an appropriately scaled form, then reads

$$E(\mathbf{M}) = d^2 \int_\Omega |\nabla \mathbf{M}|^2 \, dx + \int_{\mathbb{R}^3} |-\nabla U|^2 \, dx - 2 \int_\Omega \mathbf{H}_{\rm ext} \cdot \mathbf{M} \, dx, \tag{1}$$

cf. DeSimone et al. (2002). The stray field $\mathbf{H}_{\rm str} = -\nabla U$ is the gradient field of a potential $U\colon \mathbb{R}^3 \to \mathbb{R}$ and determined through the magnetostatic Maxwell equation

$$\nabla \cdot (\mathbf{H}_{\rm str} + \mathbf{M}\,\mathbf{1}_\Omega) = 0 \in \mathcal{D}(\mathbb{R}^3)'. \tag{2}$$

Local minimizers of the energy are (meta) stable states of the physical system. Due to the presence of both short-range ($d \ll 1$) and long-range interactions (i.e. the stray-field energy), direct numerical simulation of the full model is computationally very intense and only possible for small samples.

⋆ The first and second authors (LD, EE) acknowledge a grant from the International Max Planck Research School *Mathematics in the Sciences*. The research of the third author (SFL) is supported by the DFG via the Priority Program SPP 1239.

*Reduced Model*

In this note, we propose a modification of the reduced 2-d model by DeSimone et al. (2001) for soft ferromagnetic films under external fields, which is a description on the level of the mesoscopic in-plane magnetization $\mathbf{m}\colon \omega \to \mathbb{R}^2$. Basis for the original and our modified reduced model is the fact that in a suitable parameter regime (of thin but not too small samples, see DeSimone et al. (2002)), the in-plane divergence $\sigma = -\nabla\cdot\mathbf{m}$ is determined by a balance of magnetostatic energy and external field contribution: The magnetization $\mathbf{m}$ is a minimizer of

$$\frac{1}{4\pi} \int_\omega \int_\omega \frac{\sigma(x)\sigma(y)}{|x-y|} \, dy \, dx - 2 \int_\omega (\mathbf{H}_{\rm ext} \cdot x)\sigma \, dx$$

under the *relaxed* constraint $|\mathbf{m}| \le 1$.

However, even together with the full constraint $|\mathbf{m}| = 1$ and the boundary condition $\nu \cdot \mathbf{m} = 0$ at the boundary $\partial\omega$ of the cross section, the knowledge of $\sigma$ does *not* determine $\mathbf{m}$. This can easily be seen in case of $\sigma = 0$ (that is, for vanishing external field) where any continuous, piecewise smooth solution of the Eikonal equation $|\nabla\psi| = 1$ in $\omega$ that vanishes on $\partial\omega$ yields a solution via $\mathbf{m} = -\nabla^\perp\psi$ (i.e. $\psi$ acts as a stream function). The discontinuity lines of $\nabla\psi$ correspond to walls. One example for $\psi$ is the distance function to $\partial\omega$; it gives rise to the mesoscopic magnetization configuration called the "Landau state".

*Original Selection Criterion*

In its original version, the model by DeSimone et al. (2001) proposed a mathematically convenient but physically unjustified selection principle that consists of two steps:

1.) Determine the minimizer $\mathbf{m}^*$ of the relaxed problem with *minimal* $L^2$-norm, which is expected to be continuous (and thus does *not* capture walls). The cross section $\omega$ splits into a region with active constraint, that is $\{|\mathbf{m}^*| = 1\}$, where $\mathbf{m} = \mathbf{m}^*$ for any minimizer $\mathbf{m}$, and where the stray field no longer expels the external field and thus is called the *penetrated region*, and its complement $\{|\mathbf{m}^*| < 1\}$ which is non-empty.

2.) Determine the *unique* viscosity solution $\psi$ of the Dirichlet problem for the modified Eikonal equation

$$|(\mathbf{m}^*)^\perp + \nabla\psi| = 1 \quad \text{in } \omega, \quad \psi = 0 \quad \text{on } \partial\omega. \tag{3}$$

The viscosity solution is the pointwise supremum of all continuous, piecewise smooth solutions of (3).

Then take $\mathbf{m} = \mathbf{m}^* - \nabla^\perp\psi$ as the model prediction. Despite its lack of physical motivation, this selection principle works well in explaining some experimental observations, see (DeSimone et al., 2001, Figure 2).

*Selection Criterion by Wall Energy*

We propose a selection mechanism that instead is based on the physical wall energy. Note that on the mesoscopic level of the 2-d model in DeSimone et al. (2001), walls are discontinuity lines of $\mathbf{m}$. Locally, a wall connects two constant magnetizations $\mathbf{m}^+$ to $\mathbf{m}^-$ along a straight line with normal $\nu$. By isotropy and because the control of $\nabla \cdot \mathbf{m}$ ensures continuity of the normal component (i.e. $\nu\cdot\mathbf{m}^+ = \nu\cdot\mathbf{m}^-$), the wall energy per length $e$ only depends on the angle between $\mathbf{m}^+$ and $\mathbf{m}^-$, a dependence we write as $e = e(\frac{|\mathbf{m}^+-\mathbf{m}^-|^2}{4}) = e(\sin^2\alpha)$, where $2\alpha$ is the angle of the wall.

The function $e(\frac{|\mathbf{m}^+-\mathbf{m}^-|^2}{4})$ can be systematically derived from the 3-d model by investigating optimal planar transition layers between $\mathbf{m}^+$ and $\mathbf{m}^-$. It is well-known that these transition layers depend in a non-trivial way on the parameter regime (Hubert and Schäfer, 1998, Section 3.6). In Döring et al. (2012b), a reduced model was recently introduced that allows to evaluate $e(\frac{|\mathbf{m}^+-\mathbf{m}^-|^2}{4})$ by low-complexity numerical simulation, see Section 3.

We return to the wall-energy based selection mechanism among solutions of (3): Since $\mathbf{m}^*$ is continuous, the total wall energy of a configuration $\mathbf{m} = \mathbf{m}^* - \nabla^\perp\psi$ is given by

$$\int_{J(\nabla\psi)} e\left(\frac{|[\nabla\psi]|^2}{4}\right) dx, \tag{4}$$

where $[\nabla\psi]$ denotes the jump of $\nabla\psi$ and the integral is along the one-dimensional jump set $J(\nabla\psi)$. Hence among all $\psi$ with (3), we select those that minimize (4).

*Diffuse Interface Approximation*

The sharp-interface problem (4) is numerically not very tractable, in particular since the set of all piecewise smooth solutions of (3) is difficult to parametrize. We therefore propose a diffuse interface approximation of (4) of the type of a Ginzburg-Landau functional for gradients. For a function $g$ with $g(t) > 0$ for $t \in \mathbb{R} \setminus \{0\}$, the functional

$$G_\varepsilon(\psi) = \int_\omega \frac{\varepsilon}{2}(\Delta\psi)^2 + \frac{1}{2\varepsilon} g(1 - |(\mathbf{m}^*)^\perp + \nabla\psi|^2) dx \tag{5}$$

incorporates the constraint $|(\mathbf{m}^*)^\perp+\nabla\psi|^2 = 1$, see Section 2 and see Section 4.1 for its discretization. The functions $e$ and $g$ can be systematically related by considering 1-d transition layers, see Section 2. In particular, given a (numerical approximation) to $e$, it is possible to (numerically) determine $g$.

One might wonder what has been gained in terms of complexity with respect to the original 3-d micromagnetic model. Indeed, (5) contains a small length scale (i.e. $\varepsilon$ that governs the size of the transition layers) like the original 3-d model (i.e. the width of the wall core). First, the dimension reduction significantly reduces the number of degrees of freedom in a discretization. Second, $\varepsilon$ is a numerical parameter that has to be chosen much smaller than the size of $\omega$ but can be chosen much larger than the transition layer width in the 3-d model—while still capturing the correct wall energy.

## 2. DIFFUSE INTERFACE MODEL

In this section, we address how $g$ in the diffuse interface approximation (5) has to be chosen to approximate the wall energy (4). The heuristic argument goes as follows: Suppose that $\psi_0$ minimizes (4) and that the jump set $J(\nabla\psi_0)$ is a union of smooth curves. We consider the domain pattern locally, and hence even assume that $J(\nabla\psi_0)$ is actually a straight line, and that the continuous $\mathbf{m}^*$ is actually constant. Consider a wall corresponding to a transition of the magnetization $\mathbf{m} = \mathbf{m}^* - \nabla^\perp\psi_0$ by angle $2\alpha$. In this setting, $\alpha$ is characterized by $\frac{[\nabla\psi_0]}{2} = \sin\alpha$. A classical argument with a 1-d ansatz for $\partial_1\psi_\varepsilon$ and $\partial_2\psi_\varepsilon = \text{const.}$ yields

$$\begin{aligned}\min G_\varepsilon(\psi_\varepsilon) &= 2\int_{J(\nabla\psi_0)} \int_0^{\sin\alpha} \sqrt{g(\sin^2\alpha - t^2)} dt\, dx, \\ &\overset{s=\sin^2\alpha - t^2}{=} \int_{J(\nabla\psi_0)} \int_0^{\sin^2\alpha} (\sin^2\alpha - s)^{-1/2} \sqrt{g(s)}\, ds\, dx,\end{aligned}$$

where the min is taken over the class of 1-d transition layers.

In view of (4), we therefore seek $\widetilde{g} = \sqrt{g}$ with

$$\int_0^{\sin^2\alpha} (\sin^2\alpha - s)^{-1/2} \widetilde{g}(s)\, ds = e(\sin^2\alpha), \tag{6}$$

which is Abel's integral equation. This integral equation is well studied and we refer the reader to Gorenflo and Vessella (1991) for a detailed discussion. The solution to (6) is given by the formula

$$\widetilde{g}(y) = \frac{1}{\pi}\int_0^y (y-x)^{-1/2} e'(x)\, dx. \tag{7}$$

Moreover, the stability estimate

$$\|\widetilde{g}\|_{L^\infty} \lesssim (\|e\|_{L^\infty}^{1/2} + \|e'\|_{L^\infty}^{1/2})\|e\|_{L^\infty}^{1/2}, \tag{8}$$

see (Gorenflo and Vessella, 1991, Theorem 8.3.3.) ensures that if we have a good approximation of $e$ as input to the solution formula, then the output is a good approximation of $\widetilde{g}$. The solution formula (7) reveals how to choose $g$ such that minimizers of (5) converge to minimizers of (4) in the class (3).

For physically reasonable energy densities $e$, we have $g(-t) = g(t)$, $g(0) = 0$, and $g(t) > 0$ for $t \in \mathbb{R} \setminus \{0\}$. It is, however, not clear that the functional (4) is lower semi-continuous on the set (3), which would exclude

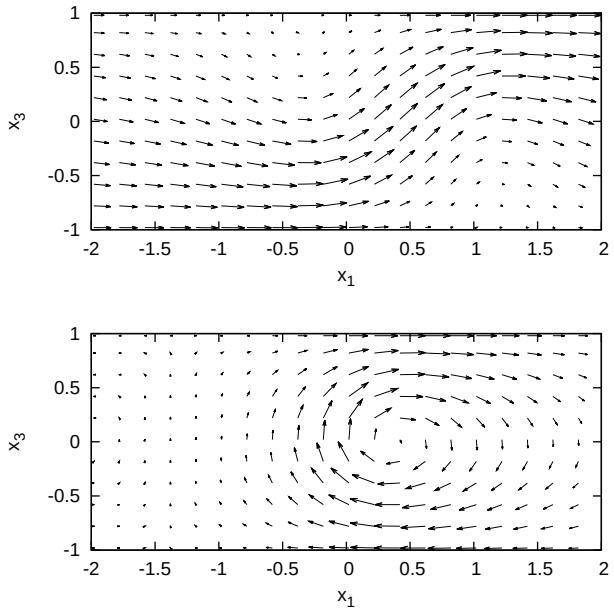


Fig. 1. Stray-field free domain walls: Asymmetric Néel (top) and asymmetric Bloch (bottom) wall.

the formation of microstructure and thus is necessary for the solvability of the variational problem. In fact, the experimental observation of a microstructure of walls (the cross-tie wall, (Hubert and Schäfer, 1998, Section 3.6.4)) has famously been explained by a lack of lower semi-continuity of (4) for a specific choice of $e$, see Alouges et al. (2002). We conjecture that for a given wall-energy density $e$, the failure of lower semi-continuity can be tested against the one-parameter family of constructions from (Alouges et al., 2002, Section 4.2.1).

But even if (4) is lower semi-continuous, e.g. in the simple case of $e(t) = Ct^{3/2}$ in which $g(t) = t^2$ and $\mathbf{m}^* = 0$, so that (5) turns into the well-studied Aviles-Giga functional, it has not been rigorously established that (5) $\Gamma$-converges to (4). This is an important open conjecture in the calculus of variations—and there are reasonable heuristics and numerics as well as lower bounds available to underline the conjecture—, see Conti and De Lellis (2007) for a discussion.

## 3. WALL ENERGY MODEL

In this section, we address the determination of the wall energy density $e$ in (4) for soft ferromagnetic films of a given exchange length $d$, cf. (1), and thickness $t$ (see Döring et al. (2012b) for a detailed discussion). In such samples, complex multiscale transition layers between domains of constant magnetization arise. They typically consist of a narrow core part of quickly rotating magnetization (cf. Figure 1), to which long, logarithmically decaying tails are attached.

While the optimal transition layer at small wall angles or in very thin films is the symmetric Néel wall, for sufficiently thick films there exists a critical wall angle $\alpha^*$ at which a supercritical bifurcation occurs and an asymmetric, stray-field free wall-core develops. As the angle further increases, the relative amount of rotation in the tails decreases.

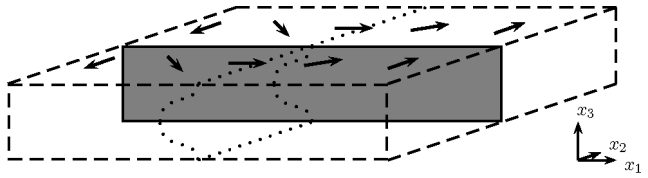


Fig. 2. The cross section of a ferromagnetic sample transversal to a domain wall. With indicated asymmetric Bloch wall.

For a rigorous analysis of this behavior we consider the Landau-Lifschitz energy (1) per length in $x_2$ on a cross section $\mathbb{R} \times (-t, t)$, transversal to the wall plane $\{x_1 = \text{const.}\}$, of an infinitely extended sample $\mathbb{R}^2 \times (-t, t)$ (cf. Figure 2). To (1) we add a uniaxial anisotropy $Q \int \mathbf{M}_1^2 + \mathbf{M}_3^2\, dx$, $Q \ll 1$, with easy axis $x_2$ as mechanism that confines the wall width, and apply the uniform external field $\mathbf{H}_{\text{ext}} = Q\big(\cos(\alpha), 0, 0\big)$. We introduce the parameters $\eta = Q(\frac{t}{d})^2$ and $\lambda = (\frac{t}{d})^2 \ln^{-1}(\frac{1}{\eta})$ and non-dimensionalize length with the film thickness $t$. Then, formally, up to an additive constant, the suitably rescaled energy of continuous transition layers $\mathbf{M} = \mathbf{M}(x_1, x_3)$ that connect the boundary values

$$\mathbf{M}(\pm\infty, \cdot) = \big(\cos(\alpha), \pm\sin(\alpha), 0\big), \tag{9}$$

is given by the expression

$$E_\eta(\mathbf{M}) = \int_{\mathbb{R}\times(-1,1)} |\nabla \mathbf{M}|^2\, dx + \lambda \ln(\tfrac{1}{\eta}) \int_{\mathbb{R}^2} |\mathbf{H}_{\text{str}}|^2\, dx + \eta \int_{\mathbb{R}\times(-1,1)} \big(\mathbf{M}_1 - \cos(\alpha)\big)^2 + \mathbf{M}_3^2\, dx,$$

where we use the notation $x = (x_1, x_3)$. The stray field $\mathbf{H}_{\text{str}}$ is determined via

$$\nabla \cdot \big(\mathbf{H}_{\text{str}} + \mathbf{M}'\, \mathbf{1}_{\mathbb{R}\times(-1,1)}\big) = 0 \in \mathcal{D}(\mathbb{R}^2)',$$

where we denote $\mathbf{M}' = (\mathbf{M}_1, \mathbf{M}_3)$.

Since the selection criterion (4) works independently of any (non-dimensional) scaling factor of $e$, we define

$$e(\sin^2 \alpha) = \min_{\mathbf{M} \text{ with } (9)} E_\eta(\mathbf{M}), \tag{10}$$

where on the right hand side the angle $\alpha$ enters through the boundary condition (9).

In the regime of small anisotropy and moderately thin films, i.e. $\eta \ll 1$ and $\lambda \sim 1$, one can prove the $\Gamma$-limit result

$$\min_{\mathbf{M} \text{ with } (9)} E_\eta(\mathbf{M}) = \min_\theta \Big( E_{\text{asym}}(\theta) + \lambda E_{\text{sym}}(\alpha - \theta) \Big) + o(1) \quad \text{as } \eta \to 0, \tag{11}$$

where

$$E_{\text{asym}}(\theta) = \min\Big\{ \int_{\mathbb{R}\times(-1,1)} |\nabla \mathbf{M}|^2 dx : \nabla \cdot \mathbf{M}' = 0 \in \mathcal{D}(\mathbb{R}^2)',\ (9) \text{ for angle } \theta \Big\}$$

denotes the energy of an asymmetric domain wall of angle $\theta$, and

$$E_{\text{sym}}(\alpha - \theta) = 2\pi \big(\cos(\theta) - \cos(\alpha)\big)^2$$

is the energy of the logarithmic tails of the Néel wall, completing the rotation from angle $\theta$ to $\alpha$. With the interpretation of $E_{\text{asym}}$ and $E_{\text{sym}}$ given above, the limit (11)

confirms that indeed domain walls consist of asymmetric wall-cores, to which logarithmically decaying tails are attached. Moreover, (11) shows that the actual size of core and tail parts in terms of the wall angle can be obtained from a 1-d minimization procedure that optimizes the energy of core and tails separately, and one can even use this reduced model to explain the supercritical bifurcation from symmetric to asymmetric walls for increasing angle $\alpha$ in sufficiently thick films.

Most important, however, for the purpose of this note is the following: Due to the exponentially decaying tails of asymmetric walls the numerical minimization of $E_{\text{asym}}$, which cannot be avoided, can be performed on small computational domains and is therefore much better tractable than direct minimization of $E_\eta$, see Section 4.2.

## 4. DISCRETIZATION AND ALGORITHMS

A discussion of the computation of the effective magnetization $\mathbf{m}^*$ is omitted and the reader is referred to Drwenski (2008); Ferraz-Leite et al. (2011); Ferraz-Leite (2011). We stress that our software is still in development. The integration of the wall-energy values into the Aviles-Giga functional is not yet implemented and we use the simplification $g(t) = t^2$, which corresponds to $e(\sin^2\alpha) = C|\sin^2\alpha|^{3/2}$, for our preliminary simulations.

### *4.1 Discretization of the Aviles-Giga Energy*

We are interested in stable states of (5). To compute critical points we therefore solve the Euler-Lagrange equation

$$\begin{aligned}&\varepsilon\int_\omega \Delta\psi\Delta\varphi\,dx+\\ &\frac{2}{\varepsilon}\int_\omega (|(\mathbf{m}^*)^\perp+\nabla\psi|^2-1)\left((\mathbf{m}^*)^\perp+\nabla\psi\right)\cdot\nabla\varphi\,dx=0\end{aligned} \tag{12}$$

for all $\varphi\in\mathcal{D}(\omega)$. In strong form it reads

$$\varepsilon\Delta^2\psi-\frac{2}{\varepsilon}\nabla\cdot\left((|(\mathbf{m}^*)^\perp+\nabla\psi|^2-1)((\mathbf{m}^*)^\perp+\nabla\psi)\right)=0, \tag{13}$$

and we prescribe essential boundary conditions

$$\psi|_{\partial\omega}=0, \partial_\nu\psi=\ell \text{ on } \partial\omega, \tag{14}$$

see Section 5.1 for a motivation of the second boundary condition $\ell$. A conforming finite element discretization of (12) must consist of continuously differentiable functions across all element interfaces. These kind of discretizations are hard to implement, and we prefer a non-conforming interior penalty method. Let $\mathcal{T}_h$ denote some regular triangulation of $\omega$ with mesh size $h$. As ansatz and test space, we use the second-order Lagrange finite-element space with incorporated Dirichlet boundary condition $\mathcal{S}_0^2(\mathcal{T}_h) := \{\Psi\in\mathcal{C}_0(\omega) : \Psi|_T \text{ is a quadratic polynomial } \forall T\in\mathcal{T}_h\}$. Let $\mathring{\mathcal{T}}_h := \bigcup_{T\in\mathcal{T}_h}\mathring{T}$ and $\partial\mathring{\mathcal{T}}_h := \bigcup_{T\in\mathcal{T}_h}\partial T\setminus\partial\omega$. To discretize the bi-Laplace operator, we define the symmetric and stabilized bilinear form

$$\begin{aligned}a(\psi,\varphi)=&\int_{\mathring{\mathcal{T}}_h}\Delta\psi\Delta\varphi\,dx-\int_{\partial\mathring{\mathcal{T}}_h}\langle\Delta\psi\rangle\,[\nabla\varphi]\,dx\\ &-\int_{\partial\mathring{\mathcal{T}}_h}[\nabla\psi]\,\langle\Delta\varphi\rangle\,dx+\frac{s}{h}\int_{\partial\mathring{\mathcal{T}}_h}[\nabla u]\,[\nabla\psi]\,dx,\end{aligned}$$

where $\langle\cdot\rangle$ denotes the mean, and $s>0$ is a sufficiently large stabilization parameter. While the boundary condition $\psi|_{\partial\omega}=0$ is incorporated into the discrete space, the boundary condition on the normal derivative, $\partial_\nu\psi=\ell$ on $\partial\omega$, is imposed weakly by Nitsche's method. The discretized version of (12), thus, reads

$$\begin{aligned}\varepsilon\Big(&a(\Psi,\Phi)-\int_{\partial\omega}\Delta\Psi(\nabla\Phi\cdot\nu)\,dx-\int_{\partial\omega}(\nabla\Psi\cdot\nu)\Delta\Phi\,dx\\ &+\frac{s}{h}\int_{\partial\omega}(\nabla\Psi\cdot\nu)(\nabla\Phi\cdot\nu)\,dx\Big)\\ &+\frac{2}{\varepsilon}\int_\omega(|(\mathbf{m}^*)^\perp+\nabla\Psi|^2-1)((\mathbf{m}^*)^\perp+\nabla\Psi)\cdot\nabla\Phi\,dx\\ &=\varepsilon\Big(-\int_{\partial\omega}\ell\Delta\Phi\,dx+\frac{s}{h}\int_{\partial\omega}\ell(\nabla\Phi\cdot\nu)\,dx\Big)\end{aligned} \tag{15}$$

for all $\Phi\in\mathcal{S}_0^2(\mathcal{T}_h)$. We solve equation (15) with a damped Newton method. The problem becomes ill-conditioned for $\varepsilon\ll 1$ and we use a nested iteration with respect to $\varepsilon$ to improve the convergence. The linear system for the Newton update is inverted with the direct sparse solver `PARDISO`, see Schenk and Gärtner (2004).

### *4.2 Computation of Wall Energies*

As outlined in Section 3, we have to determine the energy $E_{\text{asym}}(\theta)$ of asymmetric domain walls of wall angle $2\theta$ numerically. This amounts to minimization of the exchange energy of $\mathbf{M}$, subject to the linear constraint $\nabla\cdot\mathbf{M}'=0$, the non-convex constraint $|\mathbf{M}|=1$, and suitable Dirichlet boundary conditions. In contrast to the theoretical results, for practical reasons we will work on the bounded domain $[-L,L]\times(-1,1)$ with Dirichlet boundary conditions $\mathbf{M}(\pm L,\cdot)=\big(\cos(\theta),\pm\sin(\theta),0\big)$. Since exactly stray-field free domain walls have a wall width of order 1 with exponentially decaying tails, the error with respect to the solution on the unbounded domain can be expected to be small for reasonable values of $L$.

We introduce the Lagrange multipliers $\mu,p\colon B\to\mathbb{R}$ corresponding to the two constraints in $F$. The computation of critical points of the energy amounts to solving the related Euler-Lagrange equation

$$\begin{aligned}&F\left(\mathbf{M},\mu,p\right)=0,\\ &\partial_3\mathbf{M}_1=\partial_3\mathbf{M}_2=\mathbf{M}_3=0\quad\text{on }\{|x_3|=1\},\\ &\mathbf{M}=\begin{pmatrix}\cos(\theta)\\ \pm\sin(\theta)\\ 0\end{pmatrix}\quad\text{in }\{|x_1|\geq L\},\end{aligned} \tag{16}$$

with

$$F\left(\mathbf{M},\mu,p\right)=\begin{pmatrix}(-\Delta+\mu)\mathbf{M}-\nabla p\\ \frac{1}{2}(|\mathbf{M}|^2-1)\\ \nabla\cdot\mathbf{M}'\end{pmatrix}.$$

We use finite differences on a staggered grid (see Figure 3) and discretize the norm via $|\mathbf{M}|_h^2=\mathbf{M}_{1,(j_1,j_3)}^2+\mathbf{M}_{2,(j_1,j_3)}^2+\mathbf{M}_{3,(j_1,j_3)}^2$ in each cell $(j_1,j_3)$. The discrete version of (16) is then solved with a damped Newton method. Even though the Jacobians of $F$ and $F_h$ have saddle-point structure, applying the efficient direct solver `PARDISO` to the full problem in each step turned out to be faster and more robust than using an Uzawa method—at least in our implementation. The analysis of Döring et al. (2012a) reveals value and minimizer (an asymmetric Néel wall) of

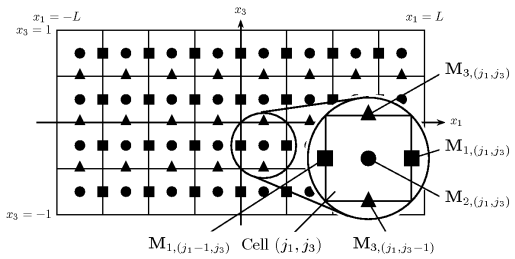


Fig. 3. The staggered grid used to discretize $E_{\mathrm{asym}}$.

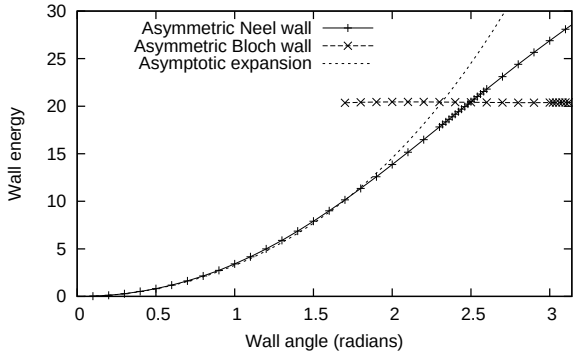


Fig. 4. The energy of asymmetric domain walls, $L = 10$, $500 \times 50$ cells in the grid.

$E_{\mathrm{asym}}$ for small wall angle to leading order explicitly. For wall angle $\pi$ a configuration of asymmetric Bloch wall type can be constructed. Using these functions as initial data leads to good convergence of the Newton method.

Figure 4 shows a plot of the energy of the wall configurations obtained by our method as well as the asymptotic expansion of $E_{\mathrm{asym}}$. Note that the latter coincides well with the numerically computed values for a remarkably large range of wall angles. Qualitatively, our results agree with the computations of Berkov et al. (1993), although in our simulation the energy of the asymmetric Bloch wall increases with decreasing wall angle. This we credit to the fact that more modern hardware enabled us to better resolve the asymmetric wall-structure, but will be object of further investigation.

## 5. MODELING AND SIMULATION OF HYSTERESIS

There is another advantage of the selection mechanism via wall energy (4) and its numerical realization via the diffuse interface approximation (5) over the selection mechanism via viscosity solution: It allows to account for some types of hysteresis, as we explain here.

### *5.1 An Additional Boundary Condition*

Note that because of $\nu \cdot \mathbf{m}^* = 0$, (3) implies for the normal derivative $\nu \cdot \nabla\psi$:

$$\nu \cdot \nabla\psi = s + \tau \cdot \mathbf{m}^* \quad \text{with } s \in \{-1, 1\} \text{ on } \partial\omega, \qquad (17)$$

where $\tau$ denotes the counter-clockwise tangent to $\partial\omega$. We claim that for any prescribed sign function $s(x)$ for $x \in \partial\omega \cap \{|\mathbf{m}^*| < 1\}$ (that is, for any point on the boundary outside the penetrated region) in (17), there are (non-viscosity) solutions of (3). This amounts to prescribing the sign in $\mathbf{m} = \mathbf{m}^* - \nabla^\perp\psi = \mp\tau$ along $\partial\omega \cap \{|\mathbf{m}^*| < 1\}$.


Fig. 5. Domain walls as simulated by the viscosity solution selection criterion for a penetrated sample. $A \in \partial\{|\mathbf{m}^*| = 1\} \cap \partial\omega$ indicates one of the transition points at the boundary from the non-saturated (plain black) to the penetrated region (striped pattern).


Fig. 6. Domain walls as simulated by the diffuse interface model. A doublet is pinned via the boundary conditions at the point $A_2$ (and symmetric on the other side). $A_1 \in \partial\{|\mathbf{m}^*| = 1\} \cap \partial\omega$ indicates one of the transition points at the boundary from the non-saturated to the penetrated region.

The heuristic argument for this existence goes as follows: Let $\partial^\pm\omega$ denote the part of $\partial\omega$ where we want to prescribe the sign $s = \pm 1$, respectively. Choose a partition of $\omega$ into two subsets $\omega^\pm$ such that $\partial\omega^\pm \cap \partial\omega = \partial^\pm\omega$; let $\psi^\pm$ denote the pointwise infimum/supremum of all continuous, piecewise smooth solutions of (3) with $\omega$ replaced by $\omega^\pm$ (hence $\psi^-$ is the viscosity solution, whereas $\psi^+$ is the anti-viscosity solution). Then the concatenation $\psi$ of $\psi^+$ and $\psi^-$ solves both (3) and (17) with the prescribed sign function $s(x)$. Note that there is no discontinuity of $\nabla\psi$ across $\partial\omega^+ \cap \partial\omega^-$. Note also that this construction fails along $\partial\omega \cap \{|\mathbf{m}^*| = 1\}$, because the distance function in the Hopf-Lax formula degenerates in the penetrated region (whose boundary $\partial\{|\mathbf{m}^*| = 1\} \cap \omega$ is characteristic), so that $\psi = 0$ on $\{|\mathbf{m}^*| = 1\}$.

Since the diffuse interface approximation (5) controls second gradients, it is also natural on the level $\varepsilon > 0$ to prescribe (inhomogeneous) Dirichlet boundary conditions for the gradient, in form of $\ell = s + \tau \cdot \mathbf{m}^*$, cf. (14).

Hence this strategy allows to numerically construct approximate minimizers $\psi$ of (4) among all functions (3) *under the additional constraint* that the sign in (17) is prescribed. This is expected to yield the optimal mesoscopic domain/wall configuration $\mathbf{m}$ *under the additional constraint* of a prescribed sign function in the boundary data $\mathbf{m} = \mp\tau$ away from the penetrated region.

### *5.2 Experiments*

In van den Berg and Vatvani (1982), the authors observed the following: Consider $\omega$ in form of a long rectangle, e.g.

of proportions $\omega = (-0.5, 0.5) \times (-0.1, 0.1)$, and apply an external field along the positive long axis. While this field is (adiabatically) increased, the original Landau pattern deforms until the field penetrates and the central wall is pushed towards the upper edge of $\omega$. Note that these events are related since the penetrated set $\{|\mathbf{m}^*| = 1\}$ is wall-free (because $\mathbf{m}^*$ is expected to be continuous). This is well-captured by the original selection criterion, cf. Figure 5.

In this process of increasing field, the penetrated part expands and point $A$ moves left. This point $A$ can be characterized in two ways:

1.) as the point $A_1$ where the boundary $\partial\{|\mathbf{m}^*| = 1\}$ of the penetrated region meets $\partial\omega$,
2.) as the point $A_2$ where the remainder of the central wall meets $\partial\omega$, cf. Figure 6, which is the point along $\partial\omega$ where $\mathbf{m}$ switches from $-\tau$ to $\tau$, a "doublet" in the language of van den Berg and Vatvani (1982).

Now the external field is reduced: Both the original model by DeSimone et al. (2001) and its modification (4) would predict exact reversal. However, in the experiment the position $A_2$ of the doublet is pinned on the way back, thus leading to hysteresis. Note that pinning is not surprising since a doublet is a point of exchange energy concentration and thus prone to be stuck at material defects.

The modification (17) is capable of modeling this pinning of the doublet, since any position of $A_2$ to the left of $A_1$ (the latter is determined solely by $\mathbf{m}^*$ and thus not affected by hysteresis) can be prescribed by describing where the jump in the sign function $s(x)$ in (17) occurs. Hence our simple model of hysteresis is that $A_2$ never moves unless forced by the constraint that it has to be to the left of $A_1$. Figure 6 shows the wall configuration that is generated by this approach on the basis of the diffuse interface approximation. In particular, a new wall segment emanates from point $A_2$, in qualitative agreement with the experiments (van den Berg and Vatvani, 1982, Fig. 9).

## 6. CONCLUSIONS

In this note, we proposed a modification of the reduced model introduced by DeSimone et al. (2001). The modification refers to the selection criterion among the solutions of the modified Eikonal equation (3). The modification consists of two parts:

1.) The criterion via the notion of viscosity solution in DeSimone et al. (2001) is replaced by a selection criterion based on physical wall energy, cf. (4).
2.) The set of admissible configurations (3) is restricted by imposing an additional boundary condition at the boundary $\partial\omega$ of the cross section, cf. (17).

To allow for a tractable numerical simulation, we furthermore proposed to replace (4) by a diffuse-interface approximation (5).

We pointed out that the main ingredient for (4), namely the wall energy $e$ as a function of the wall angle, has to capture the cross-over between different wall types depending on film thickness and wall angle. We reported on a recent reduced model that captures this cross-over, discussed its discretization and corresponding algorithms, and showed first numerical results for $e$. We showed how $e$ translates into the appropriate non-linearity $g$ in the diffuse interface approximation (5). We discussed the discretization of (5) and also presented preliminary numerical results.

Finally, we discussed how imposing the additional boundary condition, cf 2.) above, allows to capture the hysteresis observed in experiments of van den Berg and Vatvani (1982). Preliminary numerical simulation shows good qualitative agreement between our model and experiments.

## REFERENCES


Alouges, F., Rivière, T., and Serfaty, S. (2002). Néel and cross-tie wall energies for planar micromagnetic configurations. *ESAIM Control Optim. Calc. Var.*, 8, 31–68 (electronic). A tribute to J. L. Lions.

Berkov, D.V., Ramstöck, K., and Hubert, A. (1993). Solving micromagnetic problems. towards an optimal numerical method. *physica status solidi (a)*, 137(1), 207–225.

Conti, S. and De Lellis, C. (2007). Sharp upper bounds for a variational problem with singular perturbation. *Math. Ann.*, 338(1), 119–146.

DeSimone, A., Kohn, R.V., Müller, S., and Otto, F. (2002). A reduced theory for thin-film micromagnetics. *Comm. Pure Appl. Math.*, 55(11), 1408–1460.

DeSimone, A., Kohn, R.V., Müller, S., Otto, F., and Schäfer, R. (2001). Two-dimensional modelling of soft ferromagnetic films. *R. Soc. Lond. Proc. Ser. A Math. Phys. Eng. Sci.*, 457(2016), 2983–2991.

Döring, L., Ignat, R., and Otto, F. (2012a). Asymmetric domain walls of small angle in micromagnetics. In preparation.

Döring, L., Ignat, R., and Otto, F. (2012b). Cross-over from symmetric to asymmetric transition layers in micromagnetics. In preparation.

Drwenski, J. (2008). *Numerical Methods for a Reduced Model in Thin-Film Micromagnetics*. Ph.D. thesis, Rheinische Friedrichs-Willhelms-Universität Bonn.

Ferraz-Leite, S. (2011). Stabilization of a degenerate minimization problem with the simple-layer potential. Preprint, Max-Planck-Institute for Mathematics in the Sciences 84/2011.

Ferraz-Leite, S., Melenk, M., and Praetorius, D. (2011). Numerical quadratic energy minimization bound to convex constraints in thin-film micromagnetics. Accepted to Numerische Mathematik.

Gorenflo, R. and Vessella, S. (1991). *Abel integral equations*, volume 1461 of *Lecture Notes in Mathematics*. Springer-Verlag, Berlin. Analysis and applications.

Hubert, A. and Schäfer, R. (1998). *Magnetic Domains: The Analysis of Magnetic Microstructures*. Springer-Verlag, Berlin.

Landau, L. and Lifschitz, E. (1935). On the theory of the dispersion of magnetic permeability in ferromagnetic bodies. *Phys Z Sowjetunion*, 8(14), 14–22.

Schenk, O. and Gärtner, K. (2004). Solving unsymmetric sparse systems of linear equations with pardiso. *Future Gener. Comput. Syst.*, 20, 475–487.

van den Berg, H. and Vatvani, D. (1982). Wall clusters and domain structure conversions. *Magnetics, IEEE Transactions on*, 18(3), 880 – 887.